Cryogenic spin Seebeck effect

Mehrdad Elyasi [1] and Gerrit E. W. Bauer [1,2,3]
[1]*Institute for Materials Research, Tohoku University, 2-1-1 Katahira, 980-8577 Sendai, Japan*
[2]*AIMR and CSRN, Tohoku University, 2-1-1 Katahira, 980-8577 Sendai, Japan*
[3]*Zernike Institute for Advanced Materials, University of Groningen, 9747 AG Groningen, Netherlands*

(Received 16 November 2020; accepted 11 February 2021; published 24 February 2021)

We present a theory of the nonlinear spin Seebeck effect (SSE) in a ferromagnetic nanowire at cryogenic temperatures. We adopt a microscopic quantum noise model based on a collection of two-level systems. At certain positions of Pt detectors to the wire, the transverse SSE changes sign as a function of temperature and/or temperature gradient. On the other hand, the longitudinal SSE does not show significant nonlinearities even far outside the regime of validity of linear response theory.

DOI: 10.1103/PhysRevB.103.054436

I. INTRODUCTION

We address the spin Seebeck effect (SSE) in electrically insulating magnets, i.e., the spin current caused by a temperature gradient as detected by the inverse spin Hall effect voltage in heavy metal contacts [1–9]. The longitudinal SSE (LSSE) is observed in a planar configuration in which the heat and spin currents flow in parallel and normal to the interfaces [10]. The transverse, or nonlocal [11], SSE (TSSE) refers to more complicated configurations, usually two contacts on the surface of a magnetic slab or film. The spin current is injected into the metal contact by spin pumping [4], but the signal is usually dominated by the currents that are generated by temperature gradients in the bulk of the magnet [12]. The reported signals are, in general, proportional to the applied temperature differences $\triangle T$. However, several recent studies of the SSE at low temperatures [13–20] did not address a fundamental issue of thermal transport at ultralow temperatures. Linear response is valid when the perturbation is sufficiently small, but the properly normalized driving force is not $\triangle T$ but $\triangle T/T$ (or $\partial T/T$), i.e., the temperature difference divided by the average one [21]. This condition is increasingly difficult to fulfill at low temperatures, or positively formulated, it should become easier to access nonlinear thermomagnonic transport phenomena.

Existing theoretical treatments of the spin Seebeck effect are not suitable to address the low-temperature and nonlinear regimes. The low-frequency magnons that dominate at cryogenic temperatures are strongly affected by dipolar interactions, so exchange-only magnon models fail. The assumption of a semiclassical magnon accumulation in terms of a local chemical potential and magnon temperature [22] breaks down because thermalization becomes weak. With a classical magnetization noise model and in linear response, the nonthermal distribution functions governing the SSE can be described by mode-dependent (rather than position-dependent) magnon temperatures and chemical potentials [23,24]. Treatments of the stochastic magnetization dynamics in terms of classical white noise sources [25–28] do not work at low temperatures. This can be repaired by a noise spectrum that obeys the quantum fluctuation dissipation theorem [29], but at the cost of introducing phenomenological damping constants. A recent linear response study of the LSSE at low temperatures [30] focused on the magnon-polaron hybrid state at high magnetic fields [31].

The broadening of the ferromagnetic resonance of an yttrium iron garnet (YIG) sphere increases $\propto T$ for $T > 1\,\mathrm{K}$. The minimum in the damping followed by an increase and saturation with decreasing temperatures $<1\,\mathrm{K}$ [32] is caused by impurities and disorder, presumably two-level systems (TLSs) [34–36]. The spin and heat transport in this regime have, to our knowledge, not been addressed in the literature and are the focus of this paper. We study the cryogenic SSE of a ferromagnetic (FM) nanowire with a microscopic TLS model for the thermal noise, at weak magnetic fields. In this regime, magnon-magnon and magnon-phonon interactions may be safely disregarded. We predict that the antisymmetry of the TSSE signal as a function of position of a Pt detector [4,5,26] is broken in the nonlinear regime, and a nonmonotonous temperature dependence at certain contact positions emerges. These effects are caused by the nonuniform gradient of the spin distribution functions in spite of a constant temperature gradient. The LSSE signal is, on the other hand, surprisingly robust, with a linear dependence on a global temperature difference ΔT much larger than T_M.

This paper is organized as follows. Section II describes our model for the steady-state magnon dynamics of a ferromagnetic wire in the presence of temperature gradients in terms of distributed correlation functions. In Sec. III, we show the computed temperature-dependent TSSE and demonstrate why and how nonlinearities can lead to nonmonotonicity and a sign change. Section IV addresses the modification of the model from Sec. II necessary to address LSSE, followed by results. We end with a summary and a discussion of the impact and the outlook in Sec. V.

II. MODEL

In Sec. II A, we emphasize that TLSs are the main source of dissipation at very low temperatures. In Sec. II B, we introduce the magnon model interacting with a TLS ensemble that forms a thermalized reservoir. In Sec. II C, we derive the master equation of motion for the model and derive the correlation functions and their relation to the TSSE spin current.

A. Dissipation due to TLS

We consider YIG nanostructures with high-quality surfaces [33] in which scattering at low temperatures is dominated by rare earth (RE) substitutional impurities, e.g., Tb or Yb, on the Y sites [32,34–37]. Two degenerate atomic levels of a RE atom form a TLS with pseudospin $\vec{\Omega}$ that interacts with the local iron magnetic moments of spin $\vec{S}_{Fe}$ by an exchange interaction $H_{TLS} = \vec{S}_{Fe} \cdot \bar{K}\vec{\Omega}$, where $\bar{K}$ is an anisotropic exchange interaction tensor, which splits the pseudospin levels by ω_{01}. Since the RE angular momentum strongly couples to the lattice, spin waves can be efficiently dissipated via H_{TLS}. The isotropic Heisenberg exchange contribution $S_{x(y)}\Omega_{x(y)}$ couples the precessional dynamics and leads to a "transverse" relaxation that preserves the total magnetization. The anisotropy introduces "longitudinal" terms like $S_x\Omega_z$ and $S_y\Omega_z$ by which the splitting ω_{01} depends on the magnetization direction. Van Vleck [34,36] computed the lifetime broadenings due to H_{TLS} as a function of the ratio of rare earth to Fe concentration c. For the longitudinal process he reported

$$\Gamma_L = \sum_j \Gamma_{L,j} = \sum_j \frac{c_j \hbar}{6 k_B T} \sum_{n=1}^{6} \times \omega_{j,n,01}^2 f_{j,n}(\theta,\phi) \frac{\tau_{j,n}\omega_U}{1+\tau_{j,n}^2\omega_U^2}\left[1-\tanh^2\frac{\hbar\omega_{j,n,01}}{2k_BT}\right], \tag{1}$$

where j indicates a certain type of impurity or a certain corresponding TLS, while n indicates an yttrium site in the YIG unit cell. $\tau_{j,n}$ is the relaxation time of an excited TLS, $f_{j,n}(\theta,\phi) \in [0,1]$ depends on the polar magnetization direction angles θ and ϕ, and ω_U is the FMR frequency. The transverse relaxation is dominated by isotropic exchange and reads [34,36]

$$\Gamma_T = \sum_j \Gamma_{T,j} = -\mathrm{Im}\sum_j \sum_{n=1}^{6} \frac{c_j \omega_{j,n,01}}{12} \tanh\frac{\hbar\omega_{j,n,01}}{2k_BT} \times \left[\frac{\omega_U}{\omega_U - \omega_{j,n,01} + i/\tau_{j,n}} + \frac{\omega_U}{\omega_U + \omega_{j,n,01} + i/\tau_{j,n}}\right]. \tag{2}$$

For $\omega_{j,n,01} = \omega_{j,01}\,\forall n$ and $\tau_{j,n} = \tau_j\,\forall n$,

$$\Gamma_{T,j} = \frac{1}{2}\omega_U c_j \tanh\frac{\hbar\omega_{j,01}}{2k_BT} \times \begin{cases} \omega_{j,01}\tau_j/\left(1+\tau_j^2\omega_{j,01}^2\right) & \omega_{j,01} \gg \omega_U, \\ \omega_{j,01}\tau_j & \omega_{j,01} \sim \omega_U. \end{cases} \tag{3}$$

$\Gamma_{L,j}$ is a nonmonotonous function of temperature, increasing from zero at $T = 0$ up to a maximum at $\sim\hbar\omega_{01}/k_B$. $\Gamma_{T,j}$ monotonically increases from zero as T decreases and saturates to a finite value at $T = 0$ since the transverse relaxation is proportional to polarization of the TLS, i.e., $\tanh[\hbar\omega_{j,01}/(2k_BT)]/2$. The proportionality of $\Gamma_{T,j}$ with τ_j when $\omega_{j,01} \sim \omega_U$ holds only for $1/\tau_j \ll \omega_U$. $\Gamma_{T,j}$ vanishes with τ_j because of the associated lifetime broadening of the TLS density of states. Tabuchi *et al.* [32] found excellent agreement for the temperature-dependent broadening at $T < 1$ K, assuming $\omega_{01}/2\pi \sim \omega_U/2\pi \sim 10$ GHz and a temperature-independent bias. Phonon or magnon interactions vanish with temperature and cannot cause the observed increase and saturation of the broadening with decreasing temperature when $T < 1$ K. The increase in damping with temperature for $T \geqslant 1$ K could be phonon induced but could also indicate the presence of a second family of levels with larger exchange splitting. Figure 1(a) shows that the total dissipation due to the combination of two distinct TLSs, $\Gamma_{\rm tot} = \sum_{j=1,2}(\Gamma_{L,j} + \Gamma_{T,j})$, explains the observed damping very well up to $T \sim 5$ K, where we used $c_1 = 3\times10^{-7}$, $c_2 = 1\times10^{-4}$, $\tau_1 = 10$ ns, $\tau_2 = 10$ ps, $f_1 = 1$, $f_2 = 1$, $\omega_{1,01}/2\pi = 10$ GHz, and $\omega_{2,01}/2\pi = 150$ GHz. Figure 1(a) shows that at $T < 1$ K, $\Gamma_{T,1} \gg \Gamma_{L,1(2)}, \Gamma_{T,2}$. In the following, we therefore consider only a single TLS type with $\Gamma_{\rm tot} \approx \alpha_{\rm TLS}\omega_U$, where $\alpha_{\rm TLS} = c_1\tau_1\omega_{1,01}\tanh(\hbar\omega_{1,01}/2k_BT) \approx 10^{-4}$ is the (Gilbert) damping coefficient. We proceed to predict the consequence of TLS-dominated dissipation for the spin Seebeck effect. The TLS model not only captures the observed Gilbert damping at low temperature but also provides a recipe to include quantum noise and is a starting point to derive the master equation for the magnon dynamics, as detailed in Secs. II B and II C.

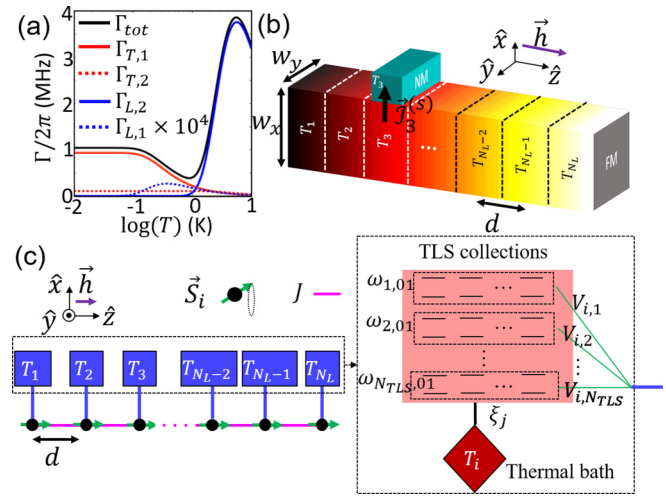

FIG. 1. Model. (a) The dissipation caused by two TLS ensembles that fit the experiments of Tabuchi *et al.* [32]. $\Gamma_{\rm tot} = \sum_{j=1,2}\Gamma_{L(T),j}$, where j indicates the ensembles parametrized by $c_1 = 3\times10^{-7}$, $c_2 = 1\times10^{-4}$, $\tau_1 = 10$ ns, $\tau_2 = 0.1$ ps, $\omega_{1,01} = 2\pi\times10$ GHz, $\omega_{2,01} = 2\pi\times150$ GHz, and $\omega_U = 2\pi\times10$ GHz. (b) A spin Seebeck current $\mathcal{J}^{(s)}$ polarized along $\hat{z}$ flows from the magnet into the metal contact. The color indicates the temperature profile, where white (black) is hottest (coldest). (c) Left: Array of spins $\vec{S}_i$, coordinate system, lattice spacing d, external magnetic field $\vec{h}$, and local reservoirs at temperature T_i. Right: Mesoreservoir of N_{TLS} two-level systems (TLS) with frequency splittings $\omega_{j,01}$. The TLS ensemble is in contact with a thermal bath (relaxation rate $\xi_j = 2\pi/\tau_j$) at temperature T_i and interacts with a spin (green lines) by $V_{i,j}$.

B. Hamiltonian

Figure 1(b) shows the schematics of the physical system, a nanowire magnetized along its length, while Fig. 1(c) shows the schematics of the corresponding spin-lattice-reservoir model. The dipolar interactions affect the magnon dispersion only for wavelengths that are much larger than the unit cell. We therefore adopt a micromagnetic approach in which the local magnetization represents an average over slices of typically 50 nm that contain many local moments. The macrospin site i then interacts with a "mesoreservoir" composed of several TLSs, as described earlier. Since the latter are local impurities with short-range exchange interactions, we may disregard their cross correlation. The mesoreservoir in turn interacts with a large reservoir with a well-defined temperature T_i that is allowed to vary slowly in space. The Hamiltonian for the model in Fig. 1(c) now reads

$$H = H_S + H_R + H_{SR}, \tag{4}$$

where H_S describes the magnet, H_R is the mesoreservoirs, and H_{SR} is the interaction between them. We expand the Heisenberg Hamiltonian for the spin chain in Fig. 1(c) to the second order of the Holstein-Primakoff transformation for a spin S on site i, i.e., $S_i^+ = \sqrt{2S}a_i^\dagger[1 - a_i^\dagger a_i/(2S)]^{1/2}$, $S_i^- = \sqrt{2S}[1 - a_i^\dagger a_i/(2S)]^{1/2}a_i$, $S_i^z = S - a_i^\dagger a_i$, in terms of magnons $a_i^\dagger$ (a_i) created (annihilated) at site i. This leads to

$$\begin{aligned} H_S = &\sum_i \left(\mathcal{A}_i - S\sum_j F_{zz}^{i,j}\right)a_i^\dagger a_i \\ &+ \sum_{i,j}\{[SJ\delta(i\pm 1, j) + \mathcal{B}_{i,j})]a_i^\dagger a_j \\ &+ \mathcal{C}_{i,j}a_i a_j + \text{H.c.}\}, \end{aligned} \tag{5}$$

where $\mathcal{A}_i = -2SJ + \gamma_e h^z$. $\mathcal{A}_{1(N_L)} = -2SJ + \gamma_e h^z$ indicates that the edges are in contact with a pinned spin; otherwise, $\mathcal{A}_{1(N_L)} = -SJ + \gamma_e h^z$. h^z is the magnetic field in the $\hat{z}$ direction; γ_e is the gyromagnetic ratio; δ is the Kronecker delta; $\mathcal{B}_{i,j} = S(F_{xx}^{i,j} + F_{yy}^{i,j})/2$; $\mathcal{C}_{i,j} = S(F_{xx}^{i,j} - F_{yy}^{i,j})/2$, where $F_{xx(yy)}^{i,j}$ is the dipolar field of S_i^x (S_i^y) exerted on S_j^x (S_j^y); and J is the exchange interaction. We compute the dipolar interactions assuming uniform dynamics along the thickness of the nanowire $\|\hat{x}$ and a nodeless cosine function amplitude with an effective width w_y' along $\hat{y}$ [38]. $F_{pp}^{i,j} = \frac{\mu_0\mu_B^2}{4\pi\hbar}\int_{V_i} d^3\vec{\rho}_i \int_{V_j} d^3\vec{\rho}_j f\, g$, where $f = \cos(\frac{\pi y_i}{w_y'})\cos(\frac{\pi y_j}{w_y'})$, $g = [1/|\vec{\rho}_{ij}|^3 - 3(p_i - p_j)^2/|\vec{\rho}_{ij}|^5]$, $p \in \{x, y\}$, $\vec{\rho}_{i(j)}$ is the position vector within site $i(j)$, $\vec{\rho}_{ij} = \vec{\rho}_i - \vec{\rho}_j$, $V_{i(j)}$ is the volume of segment $i(j)$, μ_0 is the vacuum permeability, and μ_B is the Bohr magneton.

We parametrize J by its value in the continuum limit. For long wavelengths $J = \gamma_e\mu_0 M_s\lambda^2/(d^2 S)$, where $S = NS_0$ and $N = w_x w_y d/l^3$ is the number of unit cells in each one-dimensional segment, w_x (w_y) is the thickness (width) of the nanowire, and l is the unit cell dimension. $S_0 = l^3 M_s/(2\pi\gamma_e) \approx 14$ is the net number of spins in the YIG unit cell, with magnetization $M_s = 1.46\times 10^5$ A/m, $\gamma_e = 26$ GHz/T, and $l = 1.2$ nm. The exchange length for YIG $\lambda = \sqrt{3}\times 10^{-8}$ m [39]. Figure 2(a) shows the dipolar-exchange magnon dispersion for three values of w_y, where $d = 50$ nm

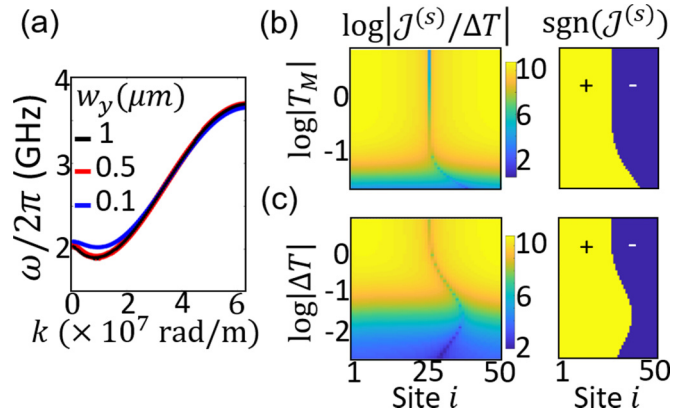

FIG. 2. (a) The magnon dispersion of a wire with different widths w_y. The wave number k corresponds to the peak of the Fourier transform of the spatial wave function. (b) and (c) Spin Seebeck current as a function of average temperature $T_M = (T_L + T_R)/2$ and temperature difference $\Delta T = T_R - T_L$, respectively. Left: $|\mathcal{J}^{(s)}/\Delta T|$. Right: $\mathcal{J}^{(s)}/|\mathcal{J}^{(s)}|$. In (b), $\Delta T = 10$ mK. In (c), $T_L = 20$ mK. In (b) and (c), $w_y = 500$ nm [red curve in (a)]. In (a)–(c), $h^z = 20$ mT.

and the number of segments $N_L = 200$, i.e., a nanowire of length $L = 10\,\mu$m. Figure 2(a) shows that the dispersion minimum becomes deeper for larger w_y. When the wire is not too narrow (e.g., $w_y > 100$ nm for $w_x = 100$ nm [38]), the dispersion relation is nonmonotonous, or "backward moving," for small wave vectors along the magnetization [40–42].

Next, we bosonize the Hamiltonian $H_R = \sum_i\sum_j \omega_{j,01} r_{i,j}^\dagger r_{i,j}$ and its interaction with the system $H_{SR} = \sum_i\sum_j (V_{i,j} r_{i,j}^\dagger a_i + \text{H.c.})$, where i labels the magnetic segments and j labels the TLS for weak excitations, i.e., $\hbar\omega_{j,01} \gg k_B T$. The TLS pseudospin Ω Hamiltonian can be simplified by another Holstein-Primakoff transformation, $\mathcal{L}_{i,j}^+ = \sqrt{2\mathcal{L}_j} r_{i,j}^\dagger$ and $\mathcal{L}_{i,j}^- = \sqrt{2\mathcal{L}_j} r_{i,j}$, where $r_{i,j}^\dagger$ ($r_{i,j}$) creates (annihilates) a boson with frequency $\omega_{j,01}$. The polarization of a TLS with index j in the collection $\mathcal{L}_j = \langle\Omega_z\rangle = \tanh[\hbar\omega_{j,01}/(2k_B T)]/2$. $V_{i,j} = \omega_{j,01}\sqrt{c_j\mathcal{L}_j}/\sqrt{S_0}$ is the interaction between a magnon on site i with pseudospin j at relative concentration c_j. Each TLS collection is in contact with a large reservoir at a (slowly varying) temperature T_i and dissipation $\xi_j = 2\pi/\tau_j$. This dissipation is accompanied by the fluctuating field acting on the TLS collection $g_{i,j} = \sqrt{\xi_j}\mathcal{F}_{i,j}$, where $\langle\mathcal{F}_{i,j}(t)\mathcal{F}_{i,j}^\dagger(t')\rangle = (n_{i,j}^{th} + 1)\delta(t - t')$, $\langle\mathcal{F}_{i,j}^\dagger\mathcal{F}_{i,j}\rangle = n_{i,j}^{th}\delta(t - t')$, and $n_{i,j}^{th} = (e^{\hbar\omega_{j,01}/k_B T_i} - 1)^{-1}$. The white noise correlation functions hold as long as $\hbar\xi_j \ll k_B T_i$ for each i, which is a safe assumption for $T_i > 10$ mK and $\tau_1 = 10$ ns. Here, we focus on low temperatures $T < 1$ K and a single TLS parametrized by $c_1 = 3\times 10^{-7}$, $\tau_1 = 10$ ns, and $\omega_{1,01}/2\pi = 10$ GHz, leading to $V_{i,1}/2\pi \approx 1.5$ MHz at $T = 0$ [see Fig. 1(a)]. We are safely in the regime $\langle r_{i,1}^\dagger r_{i,1}\rangle \ll N c_1\mathcal{L}_1$, where N is the number of unit cells, i.e., far from the saturation of TLS excitations.

C. Master equation and spin current

We now address the steady state for the model defined above, i.e., a closed system of a magnetic nanowire with a

large temperature gradient and at low temperatures. The Pt side contacts noninvasively detect the nonthermal component of site-dependent magnon distributions, i.e., the TSSE, which we compute numerically without additional approximations.

The spin Seebeck spin current can be detected by the inverse spin-Hall voltage in Pt contacts generated by the spin current pumped by a nonequilibrium magnetization at the YIG|Pt interface [4,5,43,44]. The spin pumping at site i

$$\tilde{\mathcal{J}}_i^{(SP)} \approx \frac{\hbar g_r}{4\pi}\langle \vec{S}_i \times \dot{\vec{S}}_i\rangle = \frac{\hbar g_r}{4\pi}\langle S_i^x \dot{S}_i^y - S_i^y \dot{S}_i^x\rangle, \tag{6}$$

where g_r is the real part of the complex spin-mixing conductance. We address $\mathcal{J}_i^{(SP)} = 4\pi\tilde{\mathcal{J}}_i^{(SP)}/\hbar g_r$ in the rest of the paper. $\dot{S}^{x,(y,z)} = -i[S^{x(y,z)}, H_S]$ leads to

$$\begin{aligned}\mathcal{J}_i^{(SP)} = \frac{1}{4}\sum_j \big\{ &[SJ\delta(i\pm 1, j) + \mathcal{B}_{i,j}] \\ &\times \big(\langle m_i^x m_j^x\rangle + \langle m_i^y m_j^y\rangle\big) \\ &+ \mathcal{C}_{ij}\big(-\langle m_i^x m_j^x\rangle + \langle m_i^y m_j^y\rangle\big)\big\},\end{aligned} \tag{7}$$

where $m_i^x = a_i + a_i^\dagger$, $m_i^y = -i(a_i - a_i^\dagger)$. At equilibrium, $\mathcal{J}_i^{(SP)}$ is canceled exactly by the torque induced by the thermal spin current noise emitted by the metal contact [4]. Therefore, for a certain temperature profile T_i, the net spin current pumped from site i into the nonmagnetic metal (NM) $\mathcal{J}_i^{(s)} = \mathcal{J}_i^{(SP,NEQ)} - \mathcal{J}_i^{(SP,EQ)}$, where $\mathcal{J}_i^{(SP,NEQ)}$ ($\mathcal{J}_i^{(SP,EQ)}$) are the nonequilibrium (equilibrium) currents at a contact i with temperature T_i. Disregarding any spin accumulation in the metal contacts, the SSE spin current is pumped by nonequilibrium magnons. Indeed, the dominant term (see the Appendix and Fig. 7) in $J_i^{(SP)}$ is proportional to $\langle m_i^x m_i^x\rangle + \langle m_i^y m_i^y\rangle = 4\langle a_i^\dagger a_i\rangle + 2$. Therefore, the local magnon accumulation at each site, i.e., the difference in $\langle a_i^\dagger a_i\rangle$ at equilibrium and nonequilibrium, drives the spin current $\mathcal{J}_i^{(s)}$. The thermalization is weak, so the local distribution functions cannot be parametrized by magnon temperatures or chemical potentials. We disregard the effect of the pumping on the magnon system for simplicity, which is allowed when the mixing conductance is small, e.g., for sufficiently small contacts.

The objective is the matrix Λ_∞ of the equal-time correlation function of the phase space variables $m_i^x = a_i + a_i^\dagger$, $m_i^y = -i(a_i - a_i^\dagger)$, $X_i = r_i + r_i^\dagger$, and $Y_i = -i(r_i - r_i^\dagger)$ (or symmetric covariance matrix) in the steady state that governs the spatially dependent magnon population and spin currents [see, e.g., Eq. (7)]. This is the long-time limit of the time-dependent covariance matrix Λ. Since the Hamiltonian of noninteracting magnons is quadratic and the fluctuations are Markovian, the density matrix obeys a linear master equation of motion $\dot{\Lambda} = \mathcal{O}\Lambda + \Lambda\mathcal{O} + \Upsilon$ [45], where $\dot{\mathbf{v}} = \mathcal{O}\mathbf{v} + \mathbf{c}$, $\mathbf{v} = [m_1^x, m_1^y, X_1, Y_1, \ldots, m_L^x, m_L^y, X_L, Y_L]$ and $\mathcal{O}$ is determined by the Heisenberg equation $\mathbf{v}(p) = -i[H, \mathbf{v}(p)] - \zeta(p)\mathbf{v}(p)/2$. $\zeta(p) = \xi_1$ for the phase space variables of the TLS, $p \in \{4(i-1)+3, 4(i-1)+4\}\ \forall i$, while $\zeta(p) = 0$ for the phase space variables of the magnons, $p \in \{4(i-1)+1, 4(i-1)+2\}\ \forall i$. $\mathbf{c}$ is the vector of fluctuating fields and determines $\Upsilon = \langle(\mathbf{c}^T\mathbf{c} + \mathbf{c}\mathbf{c}^T)/2\rangle$. Υ is diagonal with elements $\Upsilon(p,p) = \zeta(p)(2n_i^{th}+1) = \zeta(p)[2(e^{\hbar\omega_{1,01}/k_BT_i} - 1)^{-1} + 1]$ (n_i^{th} is the Planck distribution). We obtain Λ_∞ by solving $\mathcal{O}\Lambda_\infty + \Lambda_\infty\mathcal{O} = -\Upsilon$. The latter equation can be cast into a linear system of equations in the phase space variables that we solve numerically by inverting a (nonsparse) $(4\times N_L)^2 \times (4\times N_L)^2$ matrix, which in practice limits the system size to $N_L < 100$. The distributed spin pumping currents in Eq. (7) may then be expressed in terms of the steady-state covariance matrix Λ_∞, i.e., $\langle m_i^x m_j^x\rangle = \Lambda_\infty[4(i-1)+1, 4(j-1)+1]$ and $\langle m_i^y m_j^y\rangle = \Lambda_\infty[4(i-1)+2, 4(j-1)+2]$.

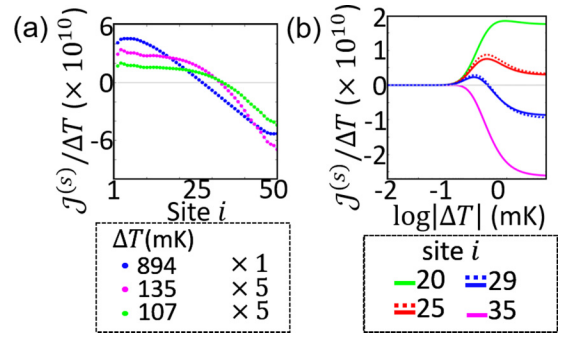

FIG. 3. (a) Site dependence of $\mathcal{J}_i^{(s)}$ for $\Delta T = 107, 135, 894$ mK from Fig. 2(c). (b) Dependence of spin current $\mathcal{J}_i^{(s)}(\Delta T)$ of four sites i on ΔT, from Fig. 2(c). The dashed lines correspond to a finer mesh $d = 25$ nm (rather than 50 nm), illustrating convergence. In (a) and (b), $T_L = 20$ mK.

Below, we calculate the TSSE by the steady-state covariance matrix as a function of the temperature gradient along the magnetic wire. In Sec. IV, we focus on the LSSE induced by temperature gradients, introducing terminal contacts that act as spin and energy sinks.

III. TSSE TEMPERATURE DEPENDENCE

We apply a linear temperature gradient with $\Delta T = T_R - T_L$; T_L (T_R) is the temperature at the left (right) edge of the nanowire. In linear response, the TSSE signal is antisymmetric, changing sign in the middle of the wire [4,5,24–26]. Figures 2(b) and 2(c) show amplitudes (left panels) and signs (right panels) of $\mathcal{J}_i^s/\Delta T$ as a function of $T_M = (T_R + T_L)/2$ and temperature difference ΔT, respectively, for $w_y = 500$ nm and $h^z = 20$ mT [with dispersion in Fig. 2(a)]. In Fig. 2(b), we show the dependence on the mean temperature T_M for fixed $\Delta T = 10$ mK. In Fig. 2(c), $T_L = 20$ mK is fixed, and the gradient ΔT is varied. According to Fig. 2(b), the signal increases with increasing T_M. The early saturation is an artifact of the frequency cutoff $\omega_{\max}$ introduced by the finite mesh size d, so results are valid for $T < \hbar\omega_{\max}/k_B$. The qualitative features nevertheless remain intact for half the mesh size d, i.e., an ∼4 times larger cutoff frequency, as illustrated in Fig. 3(b). The site index $i_\pm$ at which $\mathcal{J}_i^s$ changes sign in Fig. 2(b) shifts to the right edge with decreasing T_M below $\hbar\omega_c/k_B = 0.1$ K, where ω_c is the uniform (Kittel) mode frequency. According to Fig. 2(c), the asymmetry survives at higher temperatures with increasing temperature difference ΔT and fixed $T_L \ll \hbar\omega_c/k_B$. Figures 3(a) and 3(b) emphasize the essence of the results in Fig. 2(c) (see also the Appendix and Fig. 6). Figure 3(a) shows the deviation of the signal from an antisymmetric profile. In Fig. 3(b), we observe that for a contact on the right half of the nanowire and fixed small

$T_L = 20$ mK, the TSSE signal changes sign, and a maximum appears at relatively large ΔT and T_M. The dashed curves in Fig. 3(b) show that for smaller mesh size d, i.e., higher cutoff frequency, the peak and sign change features remain intact. For the blue curves in Fig. 3(b), the ΔT's that cause the sign change and peak are ∼0.4 and ∼0.2 K, respectively.

The deviation from an antisymmetric signal can partly be understood in a semiclassical picture. The additional occupation of a magnon mode with frequency ω_0 scales like $\delta n_{BE} \sim \tau_r v(\omega_0) \nabla n_{BE}(\omega_0)$ [12], where τ_r is a relaxation time, $v(\omega_0)$ is the group velocity, and $n_{BE}(\omega_0) = (e^{\hbar\omega_0/k_BT} - 1)^{-1}$. $\int_\omega \delta n_{BE} \neq 0$ because the magnons pile up or get drained at the edges. In linear response and a long spin-diffusion length, the dependence is linear with a zero in the center. An expansion in $\hbar\omega_0/(k_BT)$ can indicate only that $\nabla n_{BE}(\omega_0)$ is uniform for $T_M > \hbar\omega_0/k_B$ when $\Delta T \ll T_M$ [see Fig. 2(b)] and for $\Delta T \gg \hbar\omega_0/k_B$ when $T_M \sim \Delta T/2$ [see Fig. 2(c)]. A uniform $\nabla n_{BE}(\omega_0)$ leads to the antisymmetric TSSE in Figs. 2(b) and 2(c). A nonuniform $\nabla n_{BE}(\omega_0)$ breaks the antisymmetry by the spatial dependence of the magnon accumulation, which causes a substantial nonmonotonicity of the signal at certain positions.

The TSSE voltage $V_i^{(TSSE)} = 2\rho\theta_H e w_y g_r \mathcal{J}_i^s/(4\pi w_y d)$, where $-e$ is the electron charge, and for Pt, the conductivity $\rho = 0.9\,\mu\Omega$ m [46], and spin Hall angle $\theta_H = 0.07$ [47], while for the YIG/Pt interface $g_r/(w_y d) = 10^{16}$ m^{-2} [46]. This leads to $V_i^{(TSSE)} \approx 8 \times 10^{-18} \mathcal{J}_i^s$ V. The low-temperature maximum of $\mathcal{J}_i^s/\Delta T \sim 10^{10}$ for $\Delta T = 0.2$ K [see Fig. 3(b)] leads to a substantial $V_i^{(TSSE)} \sim 16$ nV.

IV. LSSE MODEL AND TEMPERATURE DEPENDENCE

The LSSE records the total spin current generated in the magnet within the spin relaxation length and not just the magnon accumulation at the contact as in the TSSE. We can access the LSSE by modifying the boundary conditions at the terminals of the wire in order to allow the spin currents to flow unimpeded into the contacts that act as spin and energy sinks. To this end, we introduce two reservoirs to the left and right of the nanowire. We assume that the reservoirs are NMs with a large spin-mixing conductance and interfacial damping, in contrast to the contacts in the TSSE, which we assumed to be noninvasive. We model the end contacts by reservoirs coupled equally to all modes in the nanowire by a structured reservoir model [45,48–50] of N_M bosonic modes, as depicted in Fig. 4. The modified total Hamiltonian $H' = H + H'_{SR}$, where $H'_{SR} = \sum_q (\mathcal{V}_{L,q} e^\dagger_{L,q} a_1 + \mathcal{V}_{R,q} e^\dagger_{R,q} a_{N_L} + \text{H.c.})$, $e^\dagger_{L(R),q}$ creates a boson in mode q of the left (right) reservoir, and $\mathcal{V}_{L(R),q}$ is the coupling of the local magnon field of the left (right) edge to the left (right) reservoir. Each boson mode in the left (right) reservoir is in contact with a large thermal bath at T_L (T_R) and dissipation ξ_L (ξ_R). This dissipation is accompanied by the fluctuating field $g'_{L(R),q} = \sqrt{\xi_{L(R)}}\mathcal{F}'_{L(R),q}$, where $\langle \mathcal{F}'_{L(R),q}(t) \mathcal{F}'^\dagger_{L(R),q}(t') \rangle = (n^{th}_{L(R),q} + 1)\delta(t - t')$, $\langle \mathcal{F}'^\dagger_{L(R),q}(t) \mathcal{F}'_{L(R),q}(t') \rangle = n^{th}_{L(R),q}\delta(t - t')$, $n^{th}_{L(R),q} = (e^{\hbar\omega_q/k_BT_{L(R)}} - 1)^{-1}$, assuming $1/\xi_{L(R)} \gg \hbar/k_BT_{L(R)}$. The density of states of the left (right) reservoir $\mathcal{G}_{L(R)}(\omega) = \sum_q 2\xi_{L(R)}\omega^2$ $[(\omega_q^2 - \omega^2)^2 + \omega^2\xi^2_{L(R)}]^{-1}$. Therefore, the dissipation of a magnon with frequency ω_q in the left (right) magnetic site to the left (right) reservoir $\Gamma'_{L(R)}(\omega_q) = \mathcal{G}_{L(R)}(\omega_q)\mathcal{V}^2_{L(R),q}$. The reservoirs should dissipate magnons of all frequencies, so we impose $N_M = N_L$ and ω_q to be frequencies of the normal magnon modes of the nanowire. The spin and energy loss at the edges is equivalent to increased damping α_{SP}, i.e., $\Gamma'_{L(R)}(\omega_q) = \alpha_{SP}\omega_q$, so $\mathcal{V}_{L(R),q} = \sqrt{\alpha_{SP}\omega_q/\mathcal{G}(\omega_q)}$. For $2\pi/\xi_{L(R)} = 10$ ns and $\alpha_{SP} = 0.1\alpha_{TLS}$, we obtain the steady-state covariance matrix Λ'_∞ as described in Sec. II C, which allows computing the spin current flowing from the left (right) reservoir into (out of) the nanowire $\mathcal{J}^{(LSSE)}_{L(R)} = -i[S^z_{1(N_L)}, H]$ as

$$\mathcal{J}^{(LSSE)}_{L(R)} = \frac{1}{2}\sum_j \big[\{SJ\delta[1(N_L) \pm 1, j] + \mathcal{B}_{1(N_L),j}\} \times \big(\langle m^x_{1(N_L)} m^y_j\rangle - \langle m^y_{1(N_L)} m^x_j\rangle\big) + \mathcal{C}_{1(N_L),j}\big(-\langle m^x_{1(N_L)} m^y_j\rangle - \langle m^y_{1(N_L)} m^x_j\rangle\big)\big]. \quad (8)$$

Figures 5(a) and 5(b) show the temperature dependence of the average current through the wire $\mathcal{J}^{(LSSE)} = (\mathcal{J}^{(LSSE)}_R - \mathcal{J}^{(LSSE)}_L)/2$. The temperature combinations in Figs. 5(a) and 5(b) are the same as in Figs. 2(b) and 2(c), i.e., fixed $\Delta T = 10$ mK but varying T_M or fixed $T_L = 20$ mK but

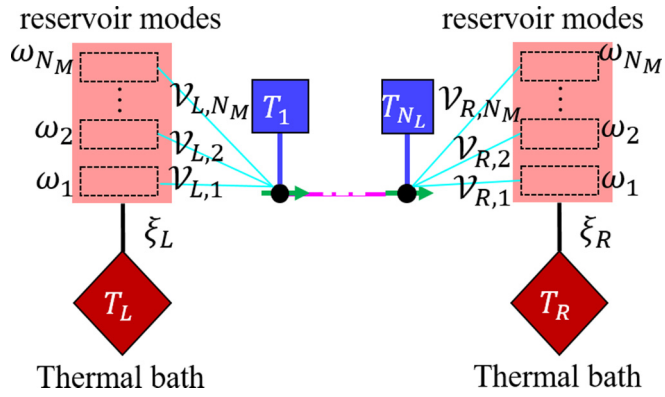

FIG. 4. The LSSE model schematics of additional mesoreservoirs to the left and right edges of the nanowire [see Fig. 1(c)]. The mesoreservoirs consist of N_M bosonic modes with frequencies ω_q and dissipate ($\xi_{L(R)}$) to a thermal bath at $T_{L(R)}$.

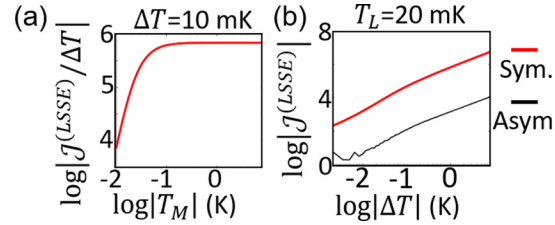

FIG. 5. Longitudinal spin Seebeck effect. The temperature dependence of the spin current at the right end point flowing into a spin sink. (a) $\Delta T = 10$ mK. (b) $T_L = 20$ mK. Here we plot $(\mathcal{J}^{(LSSE)}_L - \mathcal{J}^{(LSSE)}_R)/2$ (red line labeled Sym.) and $\mathcal{J}^{(LSSE)}_R + \mathcal{J}^{(LSSE)}_L$ (black line labeled Asym.)

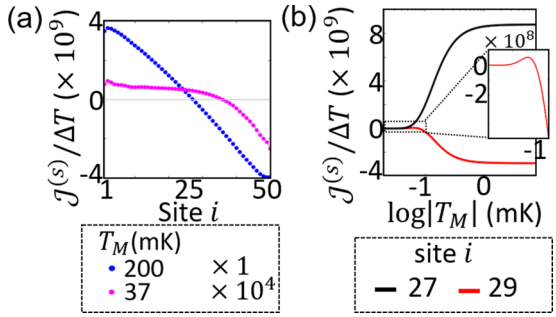

FIG. 6. (a) Site dependence of $\mathcal{J}_i^{(s)}$ for two T_M. For $T_M = 37$ mK, the plot is scaled by 10^4. (b) T_M dependence of $\mathcal{J}_i^{(s)}$ for two sites i. The inset zooms in on the maximum. In (a) and (b), $\Delta T = 10$ mK. The plots are cross sections from Fig. 2(c).

varying ΔT, respectively. Figures 5(a) and 5(b) are featureless and illustrate that even for low $T_M \ll \Delta T$, $\mathcal{J}^{(LSSE)}$ depends (quasi)linearly on ΔT [see Fig. 5(b)]. In Fig. 5(b), we also show the difference in the spin currents into the left and out of the right contacts $\mathcal{J}_R^{(LSSE)} + \mathcal{J}_L^{(LSSE)}$, which turns out to be relatively very small because LSSE is dominated by the bulk spin current, which is the same for both contacts. It should be emphasized that our TLS model is strictly valid only for $T < 1$ K.

V. CONCLUSION

We investigated SSE at cryogenic temperatures $T \lesssim 1$ K with dissipation by two-level systems. In the nonlinear temperature regime, i.e., large $\Delta T/T$, we predicted a nonmonotonic TSSE signal at a certain position of the detector contacts. For a linear temperature gradient and a contact position in the hot region, the sign changes, and a substantially large ∼10 nV voltage peak emerges at $2T_M \approx \Delta T \sim 0.2$ K. On the other hand, the LSSE signal follows a (quasi)linear dependence on ΔT, even when much larger than the average temperature. Testing our predictions will be a challenge for experiments, requiring advanced nanofabrication of magnetic insulators and state-of-the-art low-temperature equipment, but form an important step in coming to grips with magnon transport in an uncharted regime. Our model and methodology can be extended to include effects of microwave-driven coherence or spontaneous magnon condensation. Our approach provides the fluctuation statistics of the steady state in various nonequilibrium situations and at cryogenic temperatures and can be used to identify quantum squeezing and entanglement in magnonic systems.

ACKNOWLEDGMENTS

We acknowledge support from JSPS KAKENHI Grants No. 20H02609 and No. 19H006450.

APPENDIX: ADDITIONAL INFORMATION ON TSSE

Figure 6(a) shows the deviation of the TSSE current $\mathcal{J}_i^s$ from an antisymmetric profile for low T_M and $\Delta T = 10$ mK. In Fig. 6(b), we observe that for contacts on the right half of the wire the TSSE signal may change sign. Compared

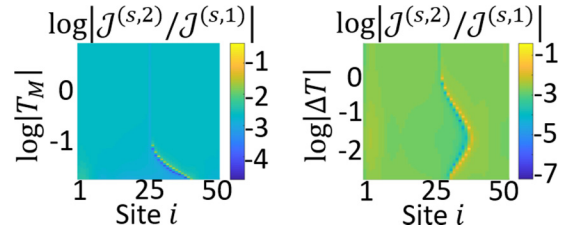

FIG. 7. $|\mathcal{J}^{(s,2)}/\mathcal{J}^{(s,1)}|$ as a function of T_M (left panel) and ΔT (right panel) for the same set of parameters as in Figs. 2(b) and 2(c), respectively.

to Fig. 3(b), this sign change and a local maximum appear at much larger ΔT and T_M, when T_L (rather than T_M) is fixed and small. Here, we estimate a TSSE voltage $V_i^{(TSSE)} \approx 8 \times 10^{-18} \mathcal{J}_i^s$ V. The low-temperature maximum in Fig. 6(b), $\mathcal{J}_i^s/\Delta T \sim 10^8$ at $\Delta T = 10$ mK, generates only a very small $V_i^{(TSSE)} \sim 8$ pV.

We support the statement in Sec. II C that magnon accumulation dominates the TSSE spin current $\mathcal{J}^{(s)}$ by the decomposition $\mathcal{J}_i^{(s)} = \mathcal{J}_i^{(s,1)} + \mathcal{J}_i^{(s,2)}$, where $\mathcal{J}^{(s,1)}$ is caused by the magnon accumulation, i.e., the difference in nonequilibrium and equilibrium values of $\langle a_i^\dagger a_i \rangle$, while $\mathcal{J}^{(s,2)}$ stands for the rest. Figure 7 shows $|\mathcal{J}_i^{(s,2)}/\mathcal{J}_i^{(s,1)}|$ as a function of T_M and ΔT for the set of parameters in Figs. 2(b) and 2(c). $|\mathcal{J}_i^{(s,2)}/\mathcal{J}_i^{(s,1)}| < 1$ proves the dominating role of the magnon accumulation.

Next, we discuss a consequence of the magnetodipolar interaction that generates negative group velocities at the origin and a minimum of the magnon dispersion at finite wave numbers. We can study the latter as a function of decreasing w_y, which causes the minimum to become shallower and finally vanish. In practice, it is convenient to modify the exchange length λ for fixed w_y, which is not physical but suffices to illustrate that the effect is small. Figure 8(a) shows the dispersion for exchange lengths $\lambda' \in \{0.5, 1, 5\}\lambda$, where λ is that of YIG. The dispersion is deeper (shallower) for smaller (larger) λ', as expected. Figure 8(b) shows the temperature dependence of $\mathcal{J}_i^{(s)}/\mathcal{J}_i'^{(s)}$ at a representative site $i = 15$, where $\mathcal{J}_i'^{(s)}$ is the TSSE current corresponding to λ'. For larger λ',

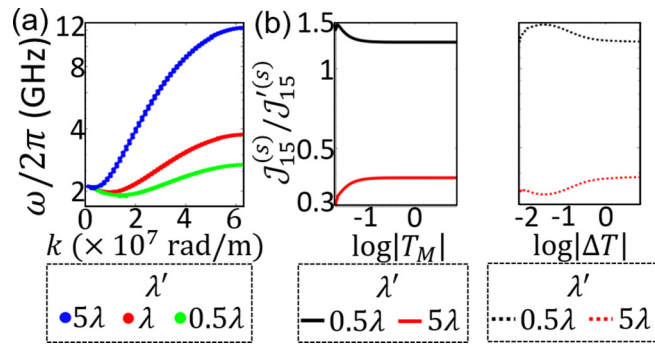

FIG. 8. (a) The magnon dispersion for three different exchange lengths, $\lambda' = 0.5\lambda$, λ, and 5λ, where λ is that of YIG. (b) Left (right): T_M (ΔT) dependence of the ratio $\mathcal{J}_i^{(s)}/\mathcal{J}_i'^{(s)}$. $\mathcal{J}_i'^{(s)}$ is the TSSE spin current for $\lambda' \neq \lambda$. The results are for site $i = 15$. In (b), vertical axes are logarithmic.

i.e., a shallower valley, the TSSE signal increases with the absolute value of the average group velocity over the occupied states. For magnetization $\|\hat{x}(\hat{y})$, the dispersion increases monotonically, which increases the spin currents, but detection by the inverse spin Hall effect becomes more complicated (not shown).

[1] K. Uchida, S. Takahashi, K. Harii, J. Ieda, W. Koshibae, K. Ando, S. Maekawa, and E. Saitoh, Nature (London) **455**, 778 (2008).

[2] K. Uchida, J. Xiao, H. Adachi, J. Ohe, S. Takahashi, J. Ieda, T. Ota, Y. Kajiwara, H. Umezawa, H. Kawai, G. E. W. Bauer, S. Maekawa, and E. Saitoh, Nat. Mater. **9**, 894 (2010).

[3] C. M. Jaworski, J. Yang, S. Mack, D. D. Awschalom, J. P. Heremans, and R. C. Myers, Nat. Mater. **9**, 898 (2010).

[4] J. Xiao, G. E. W. Bauer, K.-C. Uchida, E. Saitoh, and S. Maekawa, Phys. Rev. B **81**, 214418 (2010).

[5] H. Adachi, J.-I. Ohe, S. Takahashi, and S. Maekawa, Phys. Rev. B **83**, 094410 (2011).

[6] G. E. W. Bauer, E. Saitoh, and B. J. van Wees, Nat. Mater. **11**, 391 (2012).

[7] Y. Ohnuma, H. Adachi, E. Saitoh, and S. Maekawa, Phys. Rev. B **87**, 014423 (2013); **89**, 174417 (2014).

[8] S. M. Wu, J. E. Pearson, and A. Bhattacharya, Phys. Rev. Lett. **114**, 186602 (2015).

[9] S. M. Wu, W. Zhang, A. KC, P. Borisov, J. E. Pearson, J. S. Jiang, D. Lederman, A. Hoffmann, and A. Bhattacharya, Phys. Rev. Lett. **116**, 097204 (2016).

[10] K. Uchida, H. Adachi, T. Ota, H. Nakayama, S. Maekawa, and E. Saitoh, Appl. Phys. Lett. **97**, 172505 (2010)

[11] L. J. Cornelissen, J. Liu, R. A. Duine, J. Ben Youssef, and B. J. van Wees, Nat. Phys. **11**, 1022 (2015).

[12] S. M. Rezende, R. L. Rodríguez-Suárez, R. O. Cunha, A. R. Rodrigues, F. L. A. Machado, G. A. Fonseca Guerra, J. C. Lopez Ortiz, and A. Azevedo, Phys. Rev. B **89**, 014416 (2014).

[13] T. Kikkawa, K.-I. Uchida, S. Daimon, Z. Qiu, Y. Shiomi, and E. Saitoh, Phys. Rev. B **92**, 064413 (2015).

[14] H. Jin, S. R. Boona, Z. Yang, R. C. Myers, and J. P. Heremans, Phys. Rev. B **92**, 054436 (2015).

[15] E.-J. Guo, J. Cramer, A. Kehlberger, C. A. Ferguson, D. A. MacLaren, G. Jakob, and M. Kläui, Phys. Rev. X **6**, 031012 (2016).

[16] M. Schreier, F. Kramer, H. Huebl, S. Geprags, R. Gross, and S. T. B. Goennenwein, T. Noack, T. Langner, A. A. Serga, B. Hillebrands, and V. I. Vasyuchka, Phys. Rev. B **93**, 224430 (2016).

[17] R. Iguchi, K.-I. Uchida, S. Daimon, and E. Saitoh, Phys. Rev. B **95**, 174401 (2017).

[18] A. De, A. Ghosh, R. Mandal, S. Ogale, and S. Nair, Phys. Rev. Lett. **124**, 017203 (2020).

[19] K. Oyanagi, T. Kikkawa, and E. Saitoh, AIP Adv. **10**, 015031 (2020).

[20] K. Ganzhorn, T. Wimmer, J. Cramer, R. Schlitz, S. Geprägs, G. Jakob, R. Gross, H. Huebl, M. Kläui, and S. T. B. Goennenwein, AIP Adv. **7**, 085102 (2017).

[21] L. Onsager, Phys. Rev. **37**, 405 (1931).

[22] L. J. Cornelissen, K. J. H. Peters, G. E. W. Bauer, R. A. Duine, and B. J. van Wees, Phys. Rev. B **94**, 014412 (2016).

[23] K. Miyazakia and K. Seki, J. Chem. Phys. **108**, 7052 (1998).

[24] P. Yan, G. E. W. Bauer, and H. Zhang, Phys. Rev. B **95**, 024417 (2017).

[25] U. Ritzmann, D. Hinzke, A. Kehlberger, E.-J. Guo, M. Klaui, and U. Nowak, Phys. Rev. B **92**, 174411 (2015).

[26] J.-I. Ohe, H. Adachi, S. Takahashi, and S. Maekawa, Phys. Rev. B **83**, 115118 (2011).

[27] L. Chotorlishvili, Z. Toklikishvili, V. K. Dugaev, J. Barnas, S. Trimper, and J. Berakdar, Phys. Rev. B **88**, 144429 (2013).

[28] J. Barker and G. E. W. Bauer, Phys. Rev. Lett. **117**, 217201 (2016).

[29] J. Barker and G. E. W. Bauer, Phys. Rev. B **100**, 140401(R) (2019).

[30] R. Schmidt and P. W. Brouwer, Phys. Rev. B **103**, 014412 (2021).

[31] T. Kikkawa, K. Shen, B. Flebus, R. A. Duine, K. I. Uchida, Z. Qiu, G. E. W. Bauer, and E. Saitoh, Phys. Rev. Lett. **117**, 207203 (2016).

[32] Y. Tabuchi, S. Ishino, T. Ishikawa, R. Yamazaki, K. Usami, and Y. Nakamura, Phys. Rev. Lett. **113**, 083603 (2014).

[33] G. Schmidt, C. Hauser, P. Trempler, M. Paleschke, and E. Th. Papaioannou, Phys. Status Solidi B **2020**, 1900644 (2020).

[34] J. H. Van Vleck, J. Appl. Phys. **35**, 882 (1964).

[35] E. G. Spencer, R. C. Lecraw, and R. C. Linarks, Jr., Phys. Rev. **123**, 1937 (1961).

[36] J. H. Van Vleck and R. Orbach, Phys. Rev. Lett. **11**, 65 (1963).

[37] M. Pfirrmann, I. Boventer, A. Schneider, T. Wolz, M. Kläui, A. V. Ustinov, and M. Weides, Phys. Rev. Research **1**, 032023(R) (2019).

[38] Q. Wang, B. Heinz, R. Verba, M. Kewenig, P. Pirro, M. Schneider, T. Meyer, B. Lagel, C. Dubs, T. Bracher, and A. V. Chumak, Phys. Rev. Lett. **122**, 247202 (2019).

[39] D. D. Stancil and A. Prabhakar, *Spin Waves* (Springer, New York, 2009)

[40] M. Elyasi, Y. M. Blanter, and G. E. W. Bauer, Phys. Rev. B **101**, 054402 (2020).

[41] B. A. Kalinikos and A. N. Slavin, J. Phys. C **19**, 7013 (1986).

[42] M. J. Hurben and C. E. Patton, J. Magn. Magn. Mater. **139**, 263 (1995).

[43] S. Zhang and Z. Li, Phys. Rev. Lett. **93**, 127204 (2004).

[44] Y. Tserkovnyak, A. Brataas, and G. E. W. Bauer, Phys. Rev. Lett. **88**, 117601 (2002).

[45] H. J. Carmichael, *Statistical Methods in Quantum Optics* (Springer, Berlin, 2010).

[46] Y. Kajiwara, K. Harii, S. Takahashi, J. Ohe, K. Uchida, M. Mizuguchi, H. Umezawa, H. Kawai, K. Ando, K. Takanashi, S. Maekawa, and E. Saitoh, Nature (London) **464**, 262 (2010).

[47] L. Liu, T. Moriyama, D. C. Ralph, and R. A. Buhrman, Phys. Rev. Lett. **106**, 036601 (2011).

[48] A. J. Leggett, S. Chakravarty, A. T. Dorsey, M. P. A. Fisher, A. Garg, and W. Zwerger, Rev. Mod. Phys. **59**, 1 (1987); Erratum Rev. Mod. Phys. **67**, 725 (1995).

[49] T. Prosen, J. Stat. Mech. (2010) P07020.

[50] S. Ajisaka, F. Barra, C. Mejia-Monasterio, and T. Prosen, Phys. Rev. B **86**, 125111 (2012).